Predicting damage accumulation and fatigue life of UD composites under longitudinal tension

IOP Conf. Series: Materials Science and Engineering **388** (2018) 012007 doi:10.1088/1757-899X/388/1/012007

Predicting damage accumulation and fatigue life of UD composites under longitudinal tension

Soraia Pimenta, Alex Mersch and Marco Alves

Department of Mechanical Engineering, South Kensington Campus, Imperial College London, SW7 2AZ, United Kingdom

E-mail: soraia.pimenta@imperial.ac.uk

Abstract. Unidirectional composites under cyclic longitudinal tension develop damage through the accumulation and clustering of fibre–breaks, and through fibre–matrix interface debonding growth; these processes lead to a reduction of the material's load–carrying ability with increasing loading cycles, which raises a challenge to predict the fatigue response of composite structures. This paper proposes the first model in the literature to predict the kinetics of fibre–breakage and their effect on the macroscopic response of unidirectional composites under cyclic longitudinal tension. The model couples (i) a statistical hierarchical scaling law to predict fibre failure with (ii) a Paris law to predict interfacial fatigue damage propagating from broken fibres; due to its analytical formulation, the model predicts the response of composite bundles up to virtually any size and for their entire fatigue life in less than one minute. Model predictions for the accumulation and clustering of fibre–breaks show a good correlation with experiments from the literature; the model also predicts that, although the critical cluster size does not vary significantly between static, low–cycle/high–stress fatigue, and high–cycle/low–stress fatigue, the material can withstand the highest amount of softening under high–cycle/low–stress fatigue.

1. Introduction

Carbon–fibre composite materials are sensitive to cyclic degradation of stiffness and strength, which creates a challenge for the design of composite structures [1]. This challenge is currently addressed mostly by introducing large safety factors and/or extensive experimental campaigns, partially due to the lack of effective and efficient models to predict the accumulation of micromechanical damage with progressive cyclic loading, as well as its effect on macroscopic properties [2].

Ultimate failure of composite structures is often dominated by failure of the load–aligned plies; this makes it particularly important to develop predictive models for the cyclic response of unidirectional composites under longitudinal tension. Experimental work has shown that the load–carrying ability of carbon–fibre composites under longitudinal tension is reduced with the accumulation of loading cycles [1]. It is generally agreed that this is mostly due to degradation of matrix / interface properties with cyclic loading, since carbon–fibres are usually considered fatigue–insensitive [3].

At the micromechanical level, is is widely accepted [4] that unidirectional composites under longitudinal failure undergo accumulation and clustering of fibre–breaks, due to fibre–strength variability; this generates stress concentrations in the neighbouring fibres — at a magnitude and within a distance controlled by the properties of the matrix/interface — which might lead to further accumulation and clustering of fibre–breaks. This process can become unstable once a cluster of fibre–breaks reaches a critical size, as this triggers failure of the entire specimen.

High–resolution *in situ* micro–Computed Tomography (micro–CT) has recently demonstrated that progressive accumulation and clustering of fibre–breaks occurs under both static [5] and cyclic [6] longitudinal tension. It was also observed that cyclic loading favours the formation of small broken–clusters, and the propagation of debonds / matrix–cracks from fibre–breaks [6].

At the moment, there are no models in the literature able to predict how fibre–breaks accumulate and cluster under longitudinal tensile fatigue, nor predict the influence of this damage accumulation on the longitudinal Young's modulus. This lack of models can be justified by two factors: firstly, these are very challenging phenomena to model even under static loading [4]; secondly, most existing models for longitudinal tensile failure are too computationally demanding [4] to be applicable to fatigue loading.

We have recently developed and proposed a new approach to model longitudinal tensile failure of composites [7, 8, 9], based on a *hierarchical scaling law* defined by a statistical analysis of failure in *bundles of bundles*. This approach has allowed us to predict strength distributions and size effects for unidirectional composites under static [7] and cyclic [9] longitudinal loading, and to predict the accumulation

and clustering of fibre–breaks under static loading [8]; model predictions have been extensively validated against experiments, with blind predictions achieving an excellent correlation with independently–obtained experiments [4]. However, this approach is not yet able to predict progressive damage accumulation during fatigue loading.

Therefore, the goal of this paper is to develop this hierarchical scaling law further, to enable the prediction of the accumulation and clustering of fibre–breaks under *cyclic* longitudinal tension, and their effect on the apparent longitudinal Young's modulus of the material. An overview of the hierarchical scaling law previously developed to predict the fatigue life of unidirectional composites [9] is provided in Sections 2.1–2.3; this is then used in Sections 2.4–2.6 to predict damage accumulation under longitudinal tensile fatigue, by extending our previously proposed static formulation [8]. Model results are presented and compared against experiments in Section 3, and discussed in Section 4. Finally, Section 5 draws the main conclusions.

2. Model development

2.1. Idealisation of constituents and their constitutive laws

The model considers hierarchical fibre bundles, which are generated by paring two individual fibres (level–[0] bundles) into a level–[1] bundle, and then recursively pairing two level–$[i]$ bundles into one level–$[i+1]$ bundle (Figure 1) [7, 8, 9]. The number of fibres $n^{[i]}$ in a level-$[i]$ bundle is given by

$$n^{[i]} \stackrel{\text{def}}{=} 2^i \qquad \Leftrightarrow \qquad i = \log_2 n^{[i]}. \tag{1}$$

The fibres (with cross–section A^{f}) resist longitudinal stresses only [10] (with a longitudinal Young's modulus E^{f}) and are fatigue insensitive [3]. The strength of a single fibre under a uniform stress σ^{∞} follows a Weibull distribution with shape parameter m and scale parameter σ_0^{f}, measured at the reference length l_0^{f} [11]. Therefore, the survival probability of a single fibre ($S_{\mathrm{U}}^{[0]}$) under a uniform stress σ^{∞} can be scaled to any length l

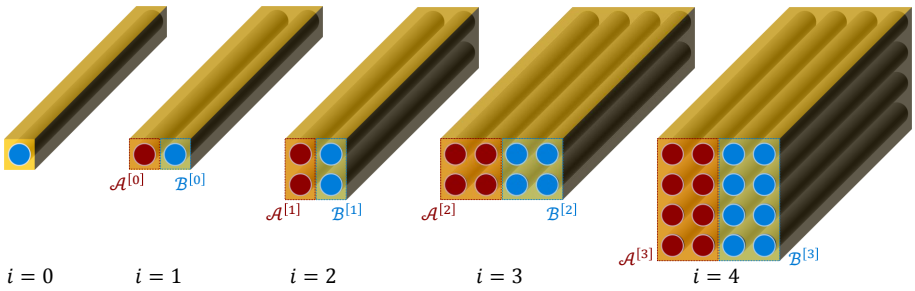

Figure 1: Hierarchical generation of composite fibre–bundles [7, 8, 9].

according to the Weakest Link Theory (WLT):

$$S_{\mathrm{U}}^{[0]}(\sigma^{\infty};l) \stackrel{\text{def}}{=} \exp\left[-\frac{l}{l_0^{\mathrm{f}}}\cdot\left(\frac{\sigma^{\infty}}{\sigma_0^{\mathrm{f}}}\right)^{m}\right]. \tag{2}$$

The fibres are embedded in a soft matrix that redistributes stresses in the neighbourhood of fibre– and sub–bundle–breaks, according to a shear-lag process [10, 12]. This shear–lag process homogenises the contributions of the matrix and fibre–matrix interface, which will hereafter be simply referred to as the *interface* between fibres and/or sub-bundles [9]. The static shear–lag response will be governed by a linear cohesive law, defined by a shear strength (τ^{int}) and mode–II fracture toughness ($\mathcal{G}_{\mathrm{IIc}}^{\mathrm{int}}$); the growth rate of mode–II interface cracks along a level–[i] sub-bundle ($\mathrm{d}A^{[i]}/\mathrm{d}N$) due to cyclic longitudinal tension of the bundle (with peak stress σ^{∞} and R–ratio R^{∞}) will be governed by a Paris law [13]:

$$\frac{\mathrm{d}A^{[i]}}{\mathrm{d}N}(\sigma^{\infty},R^{\infty}) \stackrel{\text{def}}{=} C_{\mathrm{II}}^{\mathrm{int}}\cdot\left(\frac{\Delta\mathcal{G}_{\mathrm{II}}^{[i]}(\sigma^{\infty},R^{\infty})}{\mathcal{G}_{\mathrm{IIc}}^{\mathrm{int}}}\right)^{m_{\mathrm{II}}^{\mathrm{int}}}, \text{ for } \mathcal{G}_{\mathrm{IIth}}^{\mathrm{int}} < \mathcal{G}_{\mathrm{II}}^{[i]}(\sigma^{\infty}) < \mathcal{G}_{\mathrm{IIc}}^{\mathrm{int}}, \tag{3}$$

where $C_{\mathrm{II}}^{\mathrm{int}}$ and $m_{\mathrm{II}}^{\mathrm{int}}$ are the Paris law constants, $\mathcal{G}_{\mathrm{IIth}}^{\mathrm{int}}$ is the threshold model–II energy release rate (below which no fatigue occurs), $\Delta\mathcal{G}_{\mathrm{II}}^{[i]}(\sigma^{\infty},R^{\infty}) \stackrel{\text{def}}{=} \mathcal{G}_{\mathrm{II}}^{[i]}(\sigma^{\infty}) - \mathcal{G}_{\mathrm{II}}^{[i]}(R^{\infty}\cdot\sigma^{\infty})$, and $\mathcal{G}_{\mathrm{II}}^{[i]}(\sigma)$ is the energy release rate at the level–[i] sub-bundle interface crack under a remote bundle stress σ (which will be calculated in Equation 4).

2.2. Micromechanical analysis of a level–[1] bundle under cyclic longitudinal tension

2.2.1. Static loading

Consider a level–[1] composite fibre bundle, composed of two level–[0] individual fibres bound together by a level–[0] interface, under a static uniform tensile stress field with magnitude σ^{∞}. The following scenarios may occur [7, 8, 9]:

No level–[0] breaks scenario. The bundle survives the remote peak stress σ^{∞} with both fibres undamaged, in which case there is no fatigue degradation.

Broken level–[1] bundle scenario. The bundle fails under the remote peak stress σ^{∞} (i.e. both fibres break, and an interface split forms between them), in which case no further loading is possible.

One level–[0] break scenario. The bundle survives the remote peak stress σ^{∞} with one broken fibre, while the other fibre survives the results stress concentration field created through shear of the interface (as shown in Figure 2a, with $k = 2$ from equilibrium). Depending of the mode–II energy release rate associated with crack

growth along the level–[0] sub-bundle interface

$$\mathcal{G}_{\mathrm{II}}^{[0]}(\sigma^{\infty}) \overset{[9]}{=} \frac{n^{[0]} \cdot A^{\mathrm{f}} \cdot (\sigma^{\infty})^2}{P^{[0]} \cdot E^{\mathrm{f}}} \,, \tag{4}$$

where $P^{[0]}$ is the perimeter of the level–[0] interface, two sub-scenarios may occur:

Fully–debonded scenario. If $\mathcal{G}_{\mathrm{II}}^{[0]}(\sigma^{\infty}) \geq \mathcal{G}_{\mathrm{IIc}}^{\mathrm{int}}$, an interface crack tip will form and propagate unstably during the static loading cycle, leaving the specimen *fully-debonded* (see Figure 2c);

Fatigue–sensitive scenario. If $\mathcal{G}_{\mathrm{II}}^{[i]}(\sigma^{\infty}) < \mathcal{G}_{\mathrm{IIc}}^{\mathrm{int}}$, the interface will be partially damaged near the fibre–break, within the *effective recovery length* (see Figure 2a):

$$l_{\mathrm{e}}^{[0]}(\sigma^{\infty}, N=0) \overset{[9]}{=} 2 \cdot \frac{1}{\lambda^{[0]}} \cdot \arcsin\left(\sqrt{\frac{\mathcal{G}_{\mathrm{II}}^{[0]}(\sigma^{\infty})}{\mathcal{G}_{\mathrm{IIc}}^{\mathrm{int}}}}\right) \,,$$

$$\text{where} \quad \lambda^{[0]} \overset{\text{def}}{=} \frac{\tau^{\mathrm{int}}}{\sqrt{n^{[0]} \cdot A^{\mathrm{f}}/P^{[0]} \cdot E^{\mathrm{f}} \cdot \mathcal{G}_{\mathrm{IIc}}^{\mathrm{int}}}} \,. \tag{5}$$

2.2.2. Fatigue life

Only the **fatigue–sensitive scenario** defined above is susceptible to fatigue degradation (and only if $\mathcal{G}_{\mathrm{II}}^{[0]}(\sigma^{\infty}) > \mathcal{G}_{\mathrm{IIth}}^{\mathrm{int}}$). In this scenario, a subsequent number of load cycles (N) under a loading ratio R^{∞} will lead to a bi-lateral increase of the effective recovery length governed by the mode–II Paris law of the interface [9]:

$$\frac{\mathrm{d}l_{\mathrm{e}}^{[0]}}{\mathrm{d}N}(\sigma^{\infty}, R^{\infty}, N) \overset{\text{Eq. 3}}{=} \frac{2}{P^{[0]}} \cdot \frac{\mathrm{d}A^{[0]}}{\mathrm{d}N}(\sigma^{\infty}, R^{\infty}) \,. \tag{6}$$

This growth of the effective recovery length will lead to an evolution of the stress fields within the fibres and interface of the level–[1] bundle, leading to three district fatigue phases, as will be described next.

Crack initiation phase, for $0 < N \leq N_{\mathrm{init}}^{[0]}$. Cyclic loading progressively reduces the ability of the interface to transfer shear–stresses near the fibre–break, up to the moment when a crack–tip is formed. It has been previous shown [9] that the

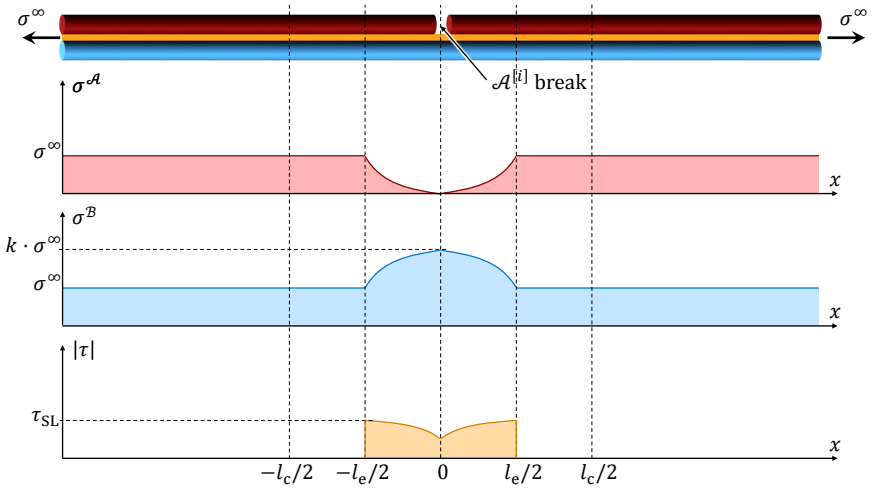

(a) During the crack–initiation phase.

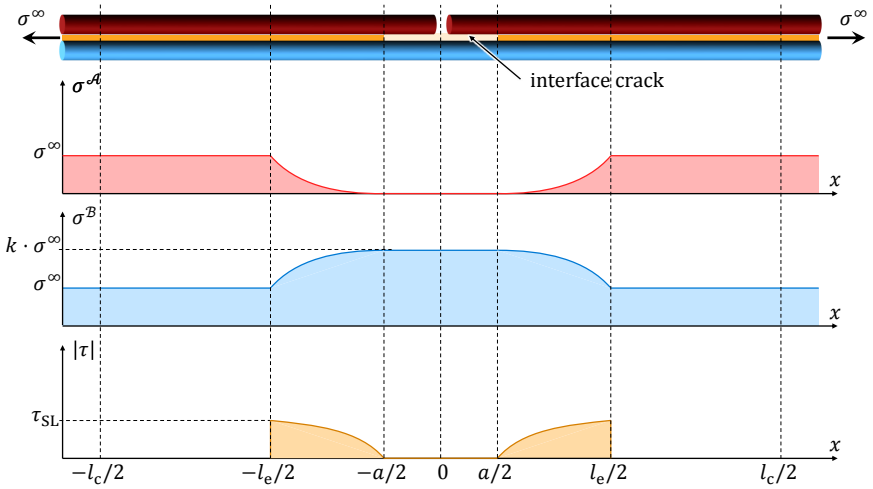

(b) During the crack–propagation phase.

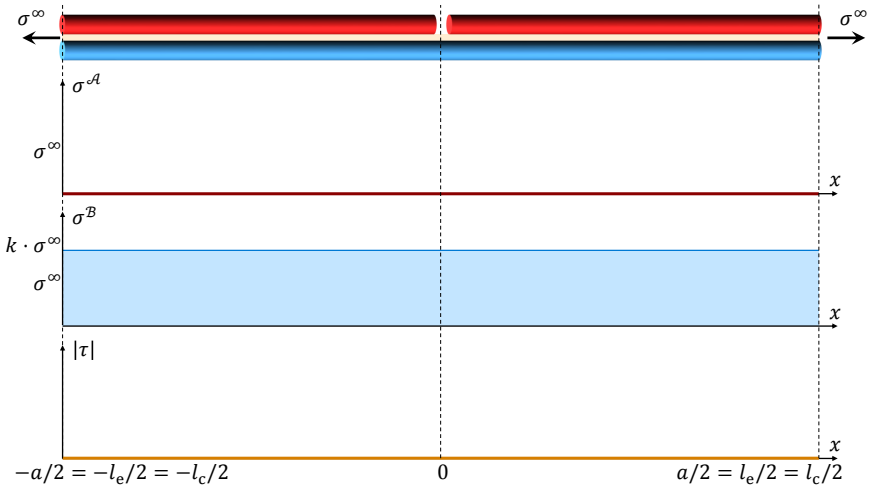

(c) After full debonding of the bundle.

Figure 2: Stress fields in the fibres and interface of a level–$[i+1=1]$ bundle, after failure of the weakest fibre (fibre $\mathcal{A}$) at $x = 0$ [9].

number of cycles required to form this crack tip is

$$N_{\text{init}}^{[0]} \overset{[9]}{=} \frac{l_{\text{K}}^{[0]} - l_{\text{e}}^{[0]}(\sigma^{\infty}, N=0)}{\dfrac{2}{P^{[0]}} \cdot \dfrac{\mathrm{d}A^{[0]}}{\mathrm{d}N}(\sigma^{\infty}, R^{\infty})}\,, \qquad \text{where } l_{\text{K}}^{[0]} \overset{\text{def}}{=} \frac{\pi}{\lambda^{[0]}}\,. \tag{7}$$

Because the formation of a crack tip marks the end of the initiation phase, the crack length is defined as $a^{[0]} = 0$ for $N \leq N_{\text{init}}^{[0]}$.

Crack propagation phase, for $N_{\text{init}}^{[0]} < N \leq N_{\text{init}}^{[0]} + \Delta N_{\text{prop}}^{[0]}$. Once an interface crack tip is formed at $N = N_{\text{init}}^{[0]}$, further cyclic loading will lead to self–similar crack propagation (see Figure 2b), up the moment when the effective recovery length reaches the end of the specimen. It has been previously shown [9] that the number of cycles required for the crack propagation phase is

$$\Delta N_{\text{prop}}^{[0]} \overset{[9]}{=} \frac{l_{\text{s}} - l_{\text{K}}^{[0]}}{\dfrac{2}{P^{[0]}} \cdot \dfrac{\mathrm{d}A^{[0]}}{\mathrm{d}N}(\sigma^{\infty}, R^{\infty})}\,. \tag{8}$$

The crack length during the propagation phase increases linearly with the number of cycles, according to the Paris law:

$$a^{[0]}(\sigma^{\infty}, R^{\infty}, N) \overset{\text{def}}{=} l_{\text{e}}^{[0]}(\sigma^{\infty}, N) - l_{\text{K}}^{[0]} \overset{\text{Eq. 6}}{=} (N - N_{\text{init}}^{[0]}) \cdot \frac{2}{P^{[0]}} \cdot \frac{\mathrm{d}A^{[0]}}{\mathrm{d}N}(\sigma^{\infty}, R^{\infty})\,. \tag{9}$$

Fully–debonded phase, for $N \geq N_{\text{init}}^{[0]} + \Delta N_{\text{prop}}^{[0]}$. Once the interface is damage along the entire length of the specimen, further crack degradation is not possible, and the stress fields in the bundle remain equal to the ones shown in Figure 2c.

2.3. Hierarchical scaling law

Considering the scenarios described in the previous section, we have previously derived [9] the following hierarchical scaling law to predict the survival probability of a level–[1] bundle (for clarity, the dependence of the survival probabilities on R^{∞} will be omitted):

$$S_{\text{U,c}}^{[1]}(\sigma^{\infty}, N) \overset{[9]}{=} S_{\mathcal{U}}^{[1]}(\sigma^{\infty}, N) + S_{\mathcal{K}}^{[1]}(\sigma^{\infty}, N)\,. \tag{10a}$$

The first term on the right–hand side of Equation 10a corresponds to the **no level**–$[i]$ **breaks scenario** (under static or fatigue loading), and can be defined as

$$S_{\mathcal{U}}^{[1]}(\sigma^{\infty},N) \overset{[9]}{=} \left[S_{\mathrm{U,e}}^{[0]}(\sigma^{\infty},N)^{\frac{l_{\mathrm{c}}^{[1]}}{l_{\mathrm{e}}^{[0]}}} \right]^{2} . \tag{10b}$$

The second term on the right–hand side of Equation 10a corresponds to the **one level**–$[i]$ **break scenario** (under static or fatigue loading), and can be defined as

$$\begin{aligned} S_{\mathcal{K}}^{[1]}(\sigma^{\infty},N) \overset{[9]}{=} 2 \cdot \left[1 - S_{\mathrm{U,e}}^{[0]}(\sigma^{\infty},N)^{\frac{l_{\mathrm{c}}^{[1]}(\sigma^{\infty},N)}{l_{\mathrm{e}}^{[0]}(\sigma^{\infty},N)}} \right] \cdot S_{\mathrm{U,e}}^{[0]}(k\cdot\sigma^{\infty},N)^{\frac{a^{[0]}(\sigma^{\infty},N)}{l_{\mathrm{e}}^{[0]}(\sigma^{\infty},N)}} \\ \cdot S_{\mathrm{K,e}}^{[0]}(\sigma^{\infty},N)^{\frac{l_{\mathrm{e}}^{[0]}(\sigma^{\infty},N)-a^{[0]}(\sigma^{\infty},N)}{l_{\mathrm{e}}^{[0]}(\sigma^{\infty},N)}} \cdot S_{\mathrm{U,e}}^{[0]}(\sigma^{\infty},N)^{\frac{l_{\mathrm{c}}^{[1]}(\sigma^{\infty},N)-l_{\mathrm{e}}^{[0]}(\sigma^{\infty},N)}{l_{\mathrm{e}}^{[0]}(\sigma^{\infty},N)}} . \end{aligned} \tag{10c}$$

The level–[0] survival probabilities in Equation 10 are calculated at the level–[0] recovery length $l_{\mathrm{e}}^{[0]}(\sigma^{\infty},N)$ (defined by Equations 5 and 6); the terms corresponding to survival probabilities under uniform stresses ($S_{\mathrm{U,e}}^{[0]}(\sigma,N)$) are directly defined by the single fibre strength distribution (Equation 2), and the term corresponding to the survival probability under non-uniform stresses ($S_{\mathrm{K,e}}^{[0]}(\sigma,N)$) is calculated based on a generalised weakest link theory [7, 9]. The resulting level–[1] survival probability is calculated at the *level*–[1] *control length* (which represents the shortest statistically independent partition of the bundle) [9]:

$$l_{\mathrm{c}}^{[1]}(\sigma^{\infty},N) \overset{[9]}{=} \min\left\{ 2\cdot l_{\mathrm{e}}^{[0]}(\sigma^{\infty},N), l_{\mathrm{s}} \right\} . \tag{11}$$

The analysis done so far focuses on a level–[1] bundle, composed of two level–[0] sub-bundles; assuming that failure propagates in a hierarchical and self–similar way in larger bundles [7, 8, 9], the hierarchical scaling law in Equation 10 can be extrapolated to any bundle of a generic level $[i+1]$ composed of two level–$[i]$ sub-bundles (with $i \geq 0$). This extrapolation requires the following modifications to the derivations shown so far:

- Replacing 'single–fibre/level–[0] sub-bundles' (and their superscript identifiers) with 'level–$[i]$ sub-bundles', and replacing 'level–[1] bundle' (and their superscript identifiers) with 'level–$[i+1]$ bundle' in Equations 4–11;

- For $i \geq 0$, replacing the standard effective recovery length (calculated in Equations 5 and 6) with the *averaged* effective recovery length, defined as [9]

$$\bar{l}_{\mathrm{e}}^{[i]}(\sigma^{\infty}, N) \overset{[9]}{=} \frac{\sum_{\eta=1}^{N} \left[l_{\mathrm{e}}^{[i]}(\sigma^{\infty}, N-\eta+1) \cdot \Delta F_{\mathrm{U,e}}^{[i]}(\sigma^{\infty}, \eta) \right]}{F_{\mathrm{U,e}}^{[i]}(\sigma^{\infty}, N)} ,$$
$$\text{where} \quad \Delta F_{\mathrm{U,e}}^{[i]}(\sigma^{\infty}, \eta) \overset{\text{def}}{=} \begin{cases} 1 - S_{\mathrm{U,e}}^{[i]}(\sigma^{\infty}, 0) & \text{for } \eta = 0, \\ S_{\mathrm{U,e}}^{[i]}(\sigma^{\infty}, \eta-1) - S_{\mathrm{U,e}}^{[i]}(\sigma^{\infty}, \eta) & \text{for } \eta \geq 1, \end{cases} \tag{12}$$

  in Equations 9 to 11. This averaging process accounts for the probability of broken clusters of level $i \geq 1$ to be formed at any fatigue cycle $N \geq 0$ (as detailed in a previous publication [9]), and will be used to calculate all effective recovery ($\bar{l}_{\mathrm{e}}$) and control ($\bar{l}_{\mathrm{c}}$) lengths hereafter.

2.4. Formation of clusters of fibre–breaks

According to the analysis done in Section 2.3, and as further detailed in a previous publication [8], the probability of having a level–$[i]$ broken–cluster in a level–$[i+1]$ bundle of length $\bar{l}_{\mathrm{c}}^{[i+1]}$ is exactly $S_{\mathcal{K}}^{[i+1]}(\sigma^{\infty}, N)$. The expected density ($\hat{\rho}_{\mathrm{clust}}^{[i]}$) of level–$[i]$ broken–clusters in a level–$[i+1]$ bundle is therefore

$$\hat{\rho}_{\mathrm{clust}}^{[i]}(\sigma^{\infty}, N) \overset{[8]}{=} \frac{S_{\mathcal{K}}^{[i+1]}(\sigma^{\infty}, N)}{\bar{V}_{\mathrm{c}}^{[i+1]}(\sigma^{\infty}, N)} , \quad \text{where } \bar{V}_{\mathrm{c}}^{[i+1]}(\sigma^{\infty}, N) \overset{\text{def}}{=} A^{[i+1]} \cdot \bar{l}_{\mathrm{c}}^{[i+1]}(\sigma^{\infty}, N) . \tag{13}$$

The total number of level–$[i]$ broken–clusters in a specimen of volume V_{s} (where the hierarchical level of the specimen is $i_{\mathrm{s}} > i+1$) will therefore correspond to performing a number $V_{\mathrm{s}}/\bar{V}_{\mathrm{c}}^{[i+1]}$ of Boolean trials with a probability of success per trial equal to $S_{\mathcal{K}}^{[i+1]}(\sigma^{\infty}, N)$. Therefore, the number of level–$[i]$ broken–clusters in the specimen is expected to follow a binomial distribution with the following expected value ($\mathbb{E}$) and variance ($\mathbb{V}$):

$$\begin{aligned} \mathbb{E}\left[N_{\mathrm{clust}}^{[i]}(\sigma^{\infty}, N) \right] &\overset{\text{def}}{=} \frac{V_{\mathrm{s}}}{\bar{V}_{\mathrm{c}}^{[i+1]}(\sigma^{\infty}, N)} \cdot S_{\mathcal{K}}^{[i+1]}(\sigma^{\infty}, N) \overset{\text{Eq. 13}}{=} \hat{\rho}_{\mathrm{clust}}^{[i]}(\sigma^{\infty}, N) \cdot V_{\mathrm{s}} \\ \mathbb{V}\left[(N_{\mathrm{clust}}^{[i]})(\sigma^{\infty}, N) \right] &\overset{\text{def}}{=} \frac{V_{\mathrm{s}}}{\bar{V}_{\mathrm{c}}^{[i+1]}(\sigma^{\infty}, N)} \cdot S_{\mathcal{K}}^{[i+1]}(\sigma^{\infty}, N) \cdot \left[1 - S_{\mathcal{K}}^{[i+1]}(\sigma^{\infty}, N) \right] \end{aligned} \tag{14a}$$

Assuming that $V_{\mathrm{s}} \gg \bar{V}_{\mathrm{c}}^{[i+1]}$ (which is usually valid for all broken–clusters with a non-negligible probability of occurrence in a macroscopic specimen), this binomial distribution of the number of broken–clusters can be approximated by a Normal

distribution with the same expected value and variance:

$$N_{\text{clust}}^{[i]}(\sigma^{\infty}, N) \sim \mathcal{N}\left(\mathbb{E}\left[N_{\text{clust}}^{[i]}(\sigma^{\infty}, N)\right],\ \mathbb{V}\left[N_{\text{clust}}^{[i]}(\sigma^{\infty}, N)\right]\right) \tag{14b}$$

2.5. Total fibre breakage

The total number of fibre–breaks in a specimen of hierarchical level i_{s} may contain contributions from broken–clusters between levels $i = 0$ (i.e. individual fibre–breaks) and $i = i_{\text{s}} - 1$ (i.e. a level–$[i_{\text{s}} - 1]$ broken–cluster) [8]. Therefore, the expected density of fibre–breaks in the specimen can be calculated as

$$\hat{\rho}_{\text{breaks}}(\sigma^{\infty}, N) \overset{[8]}{=} \sum_{i=0}^{i_{\text{s}}-1} n^{[i]} \cdot \hat{\rho}_{\text{clust}}^{[i]}(\sigma^{\infty}, N)\,. \tag{15}$$

Similarly, the total number of fibre–breaks in the level–$[i_{\text{s}}]$ specimen can be calculated by adding the contribution of all clusters:

$$N_{\text{breaks}}(\sigma^{\infty}, N) \overset{[8]}{=} \sum_{i=0}^{i_{\text{s}}-1} n^{[i]} \cdot N_{\text{clust}}^{[i]}(\sigma^{\infty}, N) \tag{16}$$

This shows that the total number of broken fibres in a specimen is a linear combination of the number of broken–clusters of all hierarchical levels $i \leq i_{\text{s}} - 1$; since the numbers of broken–clusters are normally distributed random variables (as approximated in Equation 14b), then the total number of broken fibres in a level–$[i_{\text{s}}]$ specimen follows a Normal distribution as well:

$$N_{\text{breaks}}(\sigma^{\infty}, N) \sim \mathcal{N}\left(\sum_{i=0}^{i_{\text{s}}-1} n^{[i]} \cdot \mathbb{E}\left[N_{\text{clust}}^{[i]}(\sigma^{\infty}, N)\right], \sum_{i=0}^{i_{\text{s}}-1} {n^{[i]}}^2 \cdot \mathbb{V}\left[N_{\text{clust}}^{[i]}(\sigma^{\infty}, N)\right]\right) \tag{17}$$

2.6. Strain softening under cyclic loading

Consider the different scenarios analysed in Section 2.2, but now focusing on a level–$[i{+}1]$ bundle, composed of two level–$[i]$ sub-bundles. One can impose compatibility between the expected strains in the level–$[i + 1]$ bundle ($\hat{\varepsilon}^{[i+1]}$) and those in the level–$[i]$ sub-bundles ($\hat{\varepsilon}^{[i]}$), as we have previously applied to the static loading (only) [8]; extending that approach to cyclic loading (i.e. considering the dependence of stress fields on N as

well as σ^{∞}) results in the following hierarchical scaling law:

$$\bar{\varepsilon}^{[i+1]}(\sigma^{\infty},N) \overset{[8]}{=} \left[\frac{S_{\mathcal{U}}^{[i+1]}(\sigma^{\infty},N)}{S_{\mathrm{U,c}}^{[i+1]}(\sigma^{\infty},N)}\cdot\bar{\varepsilon}_{\mathcal{U}}^{[i+1]}(\sigma^{\infty},N)+\frac{S_{\mathcal{K}}^{[i+1]}(\sigma^{\infty},N)}{S_{\mathrm{U,c}}^{[i+1]}(\sigma^{\infty},N)}\cdot\bar{\varepsilon}_{\mathcal{K}}^{[i+1]}(\sigma^{\infty},N)\right]. \tag{18a}$$

The first term on the right–hand side of Equation 18a corresponds to the **no levell**–[i] **breaks scenario** analysed in Section 2.2, which leads exclusively to linear–elastic strains. In this case, the level–[$i+1$] bundle is expected to have an average strain ($\bar{\varepsilon}_{\mathcal{U}}^{[i+1]}$) exactly equal to that of its two level–[i] sub-bundles ($\bar{\varepsilon}_{\mathcal{U}}^{\mathcal{A}^{[i]}}$ and $\bar{\varepsilon}_{\mathcal{U}}^{\mathcal{B}^{[i]}}$), imposed as follows:

$$\bar{\varepsilon}_{\mathcal{U}}^{[i+1]}(\sigma^{\infty},N) \overset{[8]}{\equiv} \bar{\varepsilon}_{\mathcal{U}}^{\mathcal{A}^{[i]}}(\sigma^{\infty},N)=\bar{\varepsilon}_{\mathcal{U}}^{\mathcal{B}^{[i]}}(\sigma^{\infty},N)=\hat{\varepsilon}^{[i]}(\sigma^{\infty},N)\,. \tag{18b}$$

The second term on the right–hand side of Equation 18a corresponds to the **one levell**–[i] **break scenario** (under static or fatigue loading) analysed in Section 2.2, and which leads to non-linear–elastic strains and to a reduction of the apparent Young's modulus. In this case, the level–[$i+1$] bundle is expected to have an average strain ($\bar{\varepsilon}_{\mathcal{K}}^{[i+1]}$) exactly equal to that of its surviving level–[i] sub-bundle $\mathcal{B}$ ($\bar{\varepsilon}_{\mathcal{K}}^{\mathcal{B}^{[i]}}$), imposed as follows:

$$\bar{\varepsilon}_{\mathcal{K}}^{[i+1]}(\sigma^{\infty},N) \overset{[8]}{\equiv} \bar{\varepsilon}_{\mathcal{K}}^{\mathcal{B}^{[i]}}(\sigma^{\infty},N)=\frac{1}{\bar{l}_{\mathrm{c}}^{[i+1]}(\sigma^{\infty},N)}\cdot\int_{x=-\bar{l}_{\mathrm{c}}^{[i+1]}(\sigma^{\infty},N)/2}^{\bar{l}_{\mathrm{c}}^{[i+1]}(\sigma^{\infty},N)/2}\hat{\varepsilon}^{[i]}(\sigma^{\mathcal{B}^{[i]}}(x),N)\,\mathrm{d}x \tag{18c}$$

Equation 18 provides a full mathematical description of a hierarchical law which scales the linear–elastic strain of single–fibres (with $\hat{\varepsilon}^{[0]}(\sigma^{\infty},N)=\sigma^{\infty}\big/E^{\mathrm{f}}$) to non-linear–elastic strains of a level–[$i+1$] bundle. The only missing element is defining and solving the integral of the non-linear–elastic term in Equation 18c; this is particularly challenging due to the following reasons:

- The solution of the integral in Equation 18c depends on the exact strain fields considered for the **one level**–[i] **break scenario** (shown in Figure 2). Therefore, the solution previously developed for *static* loading [8] is not applicable to *cyclic* loading, because the strain fields are different in the two cases;
- The stress field $\sigma^{\mathcal{B}}(x;\sigma^{\infty},N)$ in the surviving fibre/sub-bundle in the **one level**–[i] **break scenario** is continuously evolving as the number of loading cycles N increases

(as shown in Figure 2). This can be addressed by isolating the different regions of the stress field in the integral of Equation 18c:

$$\bar{\varepsilon}_{\mathcal{K}}^{[i+1]}(\sigma^{\infty},N) \overset{\text{Eq. 18c}}{=} \frac{2}{\bar{l}_{\mathrm{c}}^{[i+1]}(\sigma^{\infty},N)} \cdot \left[\int_{x=0}^{a^{[i]}(\sigma^{\infty},N)/2} \hat{\varepsilon}^{[i]}(k\cdot\sigma^{\infty},N)\,\mathrm{d}x \right. \\ + \int_{x=a^{[i]}(\sigma^{\infty},N)/2}^{\bar{l}_{\mathrm{e}}^{[i]}(\sigma^{\infty},N)/2} \hat{\varepsilon}^{[i]}(\sigma^{\mathcal{B}^{[i]}}(x),N)\,\mathrm{d}x \qquad (19a) \\ \left. + \int_{x=\bar{l}_{\mathrm{e}}^{[i]}(\sigma^{\infty},N)/2}^{\bar{l}_{\mathrm{c}}^{[i+1]}(\sigma^{\infty},N)/2} \hat{\varepsilon}^{[i]}(\sigma^{\infty},N)\,\mathrm{d}x \right] .$$

Assuming that $\hat{\varepsilon}^{[i]}(\chi\cdot\sigma,N) \approx \chi\cdot\hat{\varepsilon}^{[i]}(\sigma,N)$ (which will be verified in Section 3.3), and approximating $\sigma^{\mathcal{B}^{[i]}}(x)$ within $|x| \in [a^{[i]}/2, \bar{l}_{\mathrm{e}}^{[i]}/2]$ by a linear field, this results into

$$\bar{\varepsilon}_{\mathcal{K}}^{[i+1]}(\sigma^{\infty},N) \approx \left(1 + (k-1)\cdot\frac{a^{[i]}(\sigma^{\infty},N) + \bar{l}_{\mathrm{e}}^{[i]}(\sigma^{\infty},N)}{2\cdot\bar{l}_{\mathrm{c}}^{[i+1]}(\sigma^{\infty},N)}\right)\cdot\hat{\varepsilon}^{[i]}(\sigma^{\infty},N)\,. \qquad (19b)$$

Combining Equations 18 and 19, we can now defined the full hierarchical scaling law for the expected strains in fibre bundles under longitudinal tensile fatigue:

$$\hat{\varepsilon}^{[i+1]}(\sigma^{\infty},N) \overset{\text{Eq. 18,19}}{=} \left[\frac{S_{\mathcal{U}}^{[i+1]}(\sigma^{\infty},N)}{S_{\mathrm{U,c}}^{[i+1]}(\sigma^{\infty},N)} + \xi\cdot\frac{S_{\mathcal{K}}^{[i+1]}(\sigma^{\infty},N)}{S_{\mathrm{U,c}}^{[i+1]}(\sigma^{\infty},N)}\right]\cdot\hat{\varepsilon}^{[i]}(\sigma^{\infty},N)\,, \\ \text{where} \quad \xi \overset{\text{def}}{=} 1 + (k-1)\cdot\frac{a^{[i]}(\sigma^{\infty},N) + \bar{l}_{\mathrm{e}}^{[i]}(\sigma^{\infty},N)}{2\cdot\bar{l}_{\mathrm{c}}^{[i+1]}(\sigma^{\infty},N)}\,. \qquad (20)$$

Using the expected strains calculated in Equation 20, it is finally possible to predict degradation of the apparent longitudinal Young's modulus of a level–$[i+1]$ bundle as

$$\bar{E}^{[i+1]}(\sigma^{\infty},N) = \frac{\sigma^{\infty}}{\hat{\varepsilon}^{[i+1]}(\sigma^{\infty},N)}\,. \qquad (21)$$

3. Results

3.1. Fatigue life

Figure 3 compares the stochastic S–N curves predicted by the model against experimental results, for an unidirectional carbon/epoxy composite loaded under cyclic longitudinal tension. The input for the model (i.e. geometry of the specimens, properties of the carbon fibres, and properties of the matrices) are shown in Table 1.

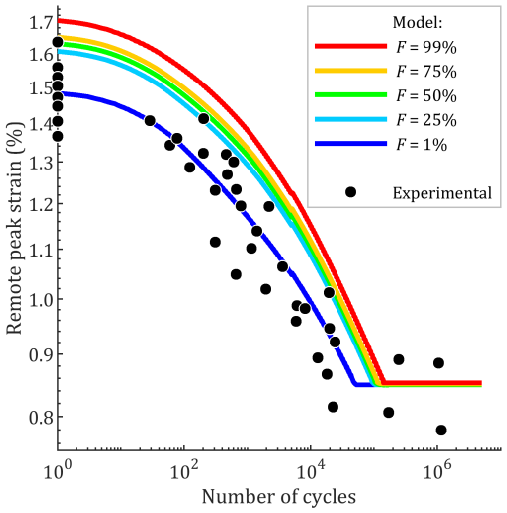

Figure 3: Stochastic S–N curves predicted by the model (for several failure probabilities F) compared against Gamstedt and Talreja's experiments [1].

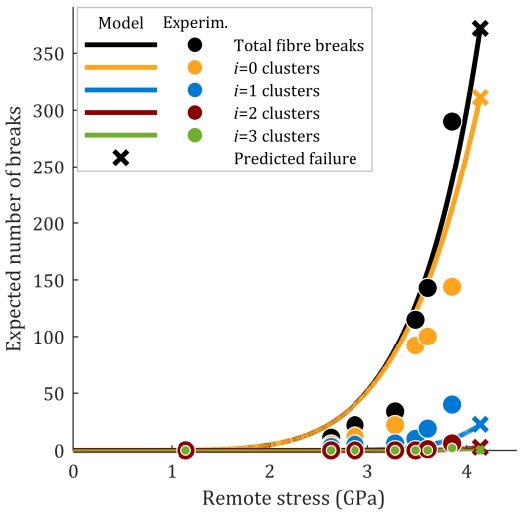

Figure 4: Static accumulation and clustering of fibre–breaks: expected values predicted by the model compared against Scott et al.'s experiments [5].

Table 1: Material properties used as model inputs for the result shown in this paper.

	Property	Units	Value	
			Gamstedt and Talreja [1]	Scott et al. [5] / Garcea et al. [6]
	Fibre type		AS4 [14]	T700 [15]
ϕ^{f}	Fibre diameter	µm	6.85	7.1
E^{f}	Fibre Young's Modulus	GPa	222	240 [16]
m	SFTT Weibull modulus		4.8	5.86
σ_0^{f}	SFTT strength paramter	GPa	4.493	7.338
l_0^{f}	SFTT gauge length	mm	10	1.0
	Matrix type / Interface		PEEK APC–2 [9]	Epoxy M21 [8]
τ^{int}	Shear strength	MPa	110	105
$\mathcal{G}_{\mathrm{IIc}}^{\mathrm{int}}$	Mode–II fracture toughness	kJ/m^2	2.0	1.0
$C_{\mathrm{II}}^{\mathrm{int}}$	Mode–II Paris law scale constant	mm^2/cycle	2×10^{-3}	3.0×10^{-3}
$m_{\mathrm{II}}^{\mathrm{int}}$	Mode–II Paris law shape constant		2.0	2.2
$\mathcal{G}_{\mathrm{IIth}}^{\mathrm{int}}$	Mode–II fatigue threshold	kJ/m^2	0.025	0.025
$n^{[i]}$	No. fibres in cross–section		100,000	5444/7577
V^{f}	Fibre volume fraction	%	60	60
l_{s}	Specimen length	mm	127	1.8/3.6
R^{∞}	Loading ratio		0.1	n.a./0.1

3.2. Accumulation and clustering of fibre breaks

Figure 4 shows the accumulation and clustering of fibre breaks in a UD carbon/epoxy specimen under increasing applied static tension. Model predictions (using the inputs shown in Table 1) are compared against experimental results obtained by Scott et al. (through *in-situ* high–resolution computed tomography [5]).

Figure 5 shows the accumulation and clustering of fibre breaks in a UD carbon/epoxy specimen under cyclic longitudinal tension. The experimental results were obtained by Garcea et al. [6] through *ex-situ* high–resolution computed tomography of the same carbon/epoxy material as analysed in Figure 4, but with a slightly different specimen geometry (see Table 1).

The evolution of the size of the largest broken cluster with the accumulation of loading cycles is shown in Figure 6, for two different remote peak stresses, comparing model predictions against experiments.

3.3. Effect of cyclic loading on apparent stiffness

Figure 7 shows the evolution of the macroscopic longitudinal strain (Figure 7a) and apparent modulus (Figure 7b) of the same carbon/epoxy specimen analysed in Section 3.2, as predicted by the model.

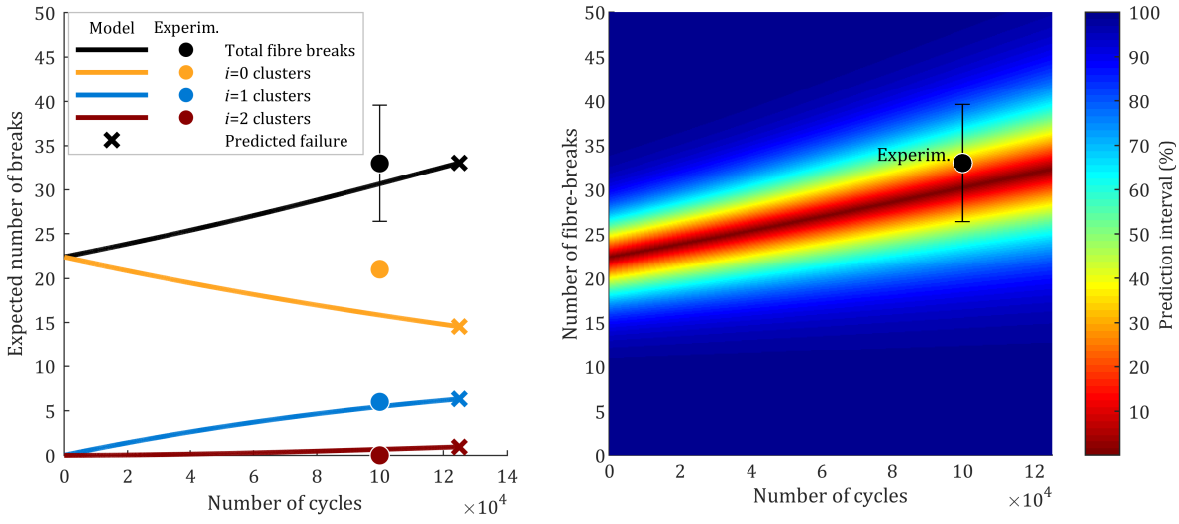

(a) Expected number of single–fibre and cluster breaks.

(b) Stochastic distribution of the total number of breaks.

Figure 5: Accumulation and clustering of fibre–breaks under cyclic loading with a remote peak load equal to 50% of the static strength. The experimental data shown was obtained by Garcea et al. [6].

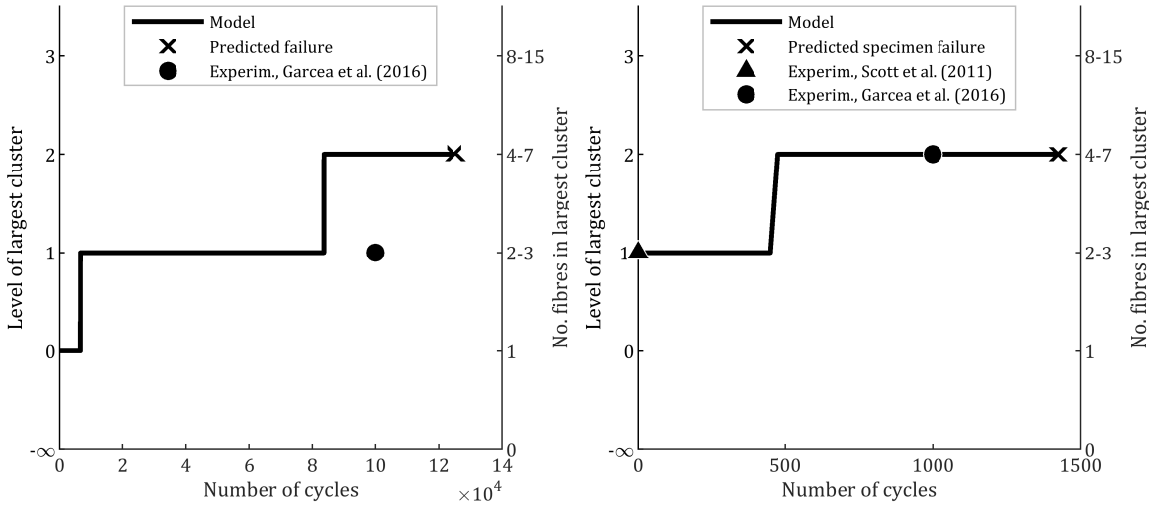

(a) Peak remote stress for cyclic load: 50% of static strength (see full distribution of fibre–breakage in Figure 5).

(b) Peak remote stress for cyclic load: 70% of static strength.

Figure 6: Evolution of the largest cluster size with cyclic loading: model predictions vs. experimental data [5, 6].

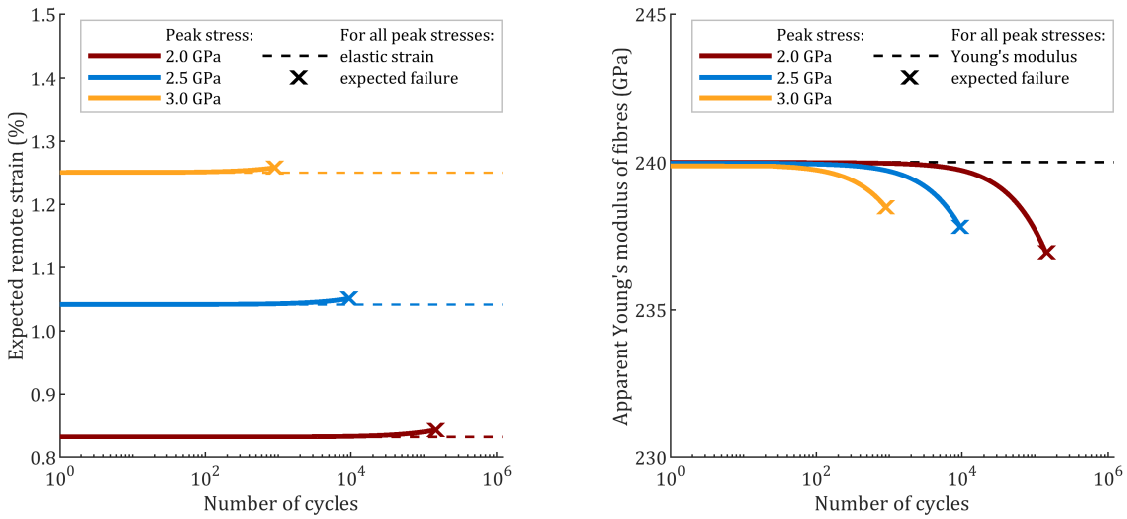

(a) Evolution of strain.

(b) Evolution of apparent modulus.

Figure 7: Effect of cyclic loading on the apparent stiffness of a carbon–epoxy composite system.

4. Discussion

4.1. Insight on the accumulation of damage in UD composites under cyclic longitudinal tension

The model proposed in this paper provides the following insight on the accumulation of damage in UD composites under cyclic longitudinal tension:

(i) The model predicts an increase of the overall density of fibre–breaks with progressive cyclic loading (Figure 5); this is due to the formation of new fibre–breaks near those previously formed during the first (i.e. static) loading cycle. Nevertheless, the total number of fibre–breaks at the moment of failure is predicted to be higher under static loading (Figure 4) than under high–cycle/low–stress fatigue (Figure 5);

(ii) The density of individual fibre–breaks decreases with progressive cyclic loading, but the density of clusters with 2–7 broken fibres increases (Figure 5a). This reveals that the kinetics of fibre–breakage under low–stress/high–cycle fatigue (where more than half of the total number of fibre–breaks is due clusters) is significantly different from that under static loading (where the large majority of the total number of fibre–breaks is due to individual/uncorrelated broken fibres, as shown in Figure 4);

(iii) The size of the largest cluster in the composite increases with progressive loading cycles (as shown in Figure 6). Interestingly, the largest cluster at the moment of failure is predicted to have the same number of fibres (4–7, i.e. level $i = 2$) under static conditions [8], low–cycle/high-stress fatigue (Figure 6b), and high–cycle/low–stress fatigue (Figure 6a).

(iv) Although extensive fibre–breakage occurs during cyclic longitudinal tension (Figure 5), this leads to a very limited reduction of the apparent modulus of the material (lower than 2%), as shown in Figure 7. This is because no large broken clusters are formed (as shown in Figure 6), and the increase of compliance due to individual fibre–breaks and small clusters is very local (i.e. limited to their effective recovery length);

(v) The loss of apparent stiffness at the moment of failure increases as one moves from low–cycle fatigue (see curve for $\sigma^{\infty} = 3.0$ GPa in Figure 7b) to high–cycle fatigue (see curve for $\sigma^{\infty} = 2.0$ GPa in Figure 7b). This suggests that unidirectional composites under longitudinal tension can accumulate larger amounts of overall damage under high–cycle/low–stress fatigue than under static loading and low–cycle/high–stress fatigue;

(vi) Combining the information from points (i), (iii), and (v) above, one can conclude that the main source of softening during fatigue loading cannot be the increase in the number of fibre–breaks or the size of broken–clusters; instead, the decrease

of apparent modulus during cyclic loading seems to be due to the increase of the effective recovery length which occurs due to mode–II fatigue of the interface near broken–fibres and clusters.

4.2. Validation of model predictions

Figures 5 and 6 show a good agreement between model predictions and experimental data. Nevertheless, the model predicts a large amount of variability for the total number of fibre breaks (see Figure 5b); this means that experimental data obtained with one specimen [5, 6] only is not sufficient to fully validate the model.

Moreover, while the model presented in this paper focuses on damage accumulation during cyclic loading, it is clear that the results will depend on the predictions of the model during the first loading cycle — i.e. under static conditions. For instance, Figure 4 suggests that the model overpredicts the density of fibre breaks under an applied stress between 60 and 80% of the static tensile strength; therefore, a similar overestimation can also been predicted for the number of fibre–breaks under cyclic loading at 70% of the static strength.

Regarding the effect of cyclic tension on the apparent Young's modulus of UD composites, it is widely accepted that UD composites under longitudinal tension present (*nearly*) no stiffness degradation under fatigue [1, 3]; this is corroborated by the predictions of the model shown in Figure 7b. A quantitative validation of the (small) stiffness degradation predicted by the model would require experimental data which, at the moment, is not available.

5. Conclusions

This paper proposed the first model in the literature to predict the kinetics of fibre–breakage and their effect on the macroscopic response of unidirectional composite materials under cyclic longitudinal tension. The following conclusions were reached:

- The model is based on the *analytical* evaluation of stress fields near fibre breaks, on a *hierarchical* statistical scaling law [7, 8], and on an *adaptive cycle jump* strategy for the fatigue analysis [9]. These features make the model capable of predicting damage accumulation in composite specimens with virtually any number of fibres and for their entire lifetime in less than 60 seconds;
- Model predictions for the accumulation and clustering of fibre–breaks under cyclic loading were successfully validated against experimental results from high–resolution computed tomography;
- The model suggests that cyclic loading leads to accumulation and clustering of fibre–breaks; however, the the critical cluster size does not vary significantly between

static, low–cycle/high–stress fatigue, and high–cycle/low–stress fatigue types of loading;

- The model suggests that unidirectional composites under longitudinal tension are able to undergo more softening under high–cycle/low–stress fatigue than under low–cycle/high–stress or static loading; this is mostly due to progressive degradation of the matrix/interface near fibre–fibres with cyclic loading.

Due to its computational efficiency and its easy–to–use analytical implementation, we expect that this model can have the following applications:

- Guiding the development of composite materials less sensitive to cyclic degradation (e.g. by predicting the effect that modifying fibre, matrix and/or interfacial properties would have on the accumulation of damage throughout the fatigue life);
- Developing macro–scale health–monitoring strategies for unidirectional composites under cyclic loading (e.g. by defining a critical value for the loss of longitudinal Young's modulus, after which the material may be prone to fatigue failure);
- Defining acceptable levels of micromechanical damage in composite structures under cyclic loading.

Acknowledgements

The research leading to these results has been done within the framework of the FiBreMoD project and has received funding from the European Union's Horizon 2020 research and innovation programme under the Marie Sklodowska–Curie grant agreement no. 722626. S. Pimenta also acknowledges the support from the Royal Academy of Engineering in the scope of her Research Fellowship on *Multiscale discontinuous composites for large scale and sustainable structural applications* (2015–2019).

The authors acknowledge Ian Sinclair from the University of Southampton and Serafina Garcea from the University of Manchester for discussions on the high–resolution computed tomography experiments.

Supporting data and the MATLAB® implementation can be requested from the corresponding author.

References

[1] E. K. Gamstedt and R. Talreja. Fatigue damage mechanisms in unidirectional carbon–fibre–reinforced plastics. *J Mater Sci*, 34(11):2535–2546, 1999.

[2] S. M. O. Tavares and P. M. S. T. de Castro. An overview of fatigue in aircraft structures. *Fatigue Fract Eng M*, 40:1510–1529, 2017.

[3] A. Somer and A. Bunsell. The tensile and fatigue behaviour of carbon fibres. *Plast Rub Compos Proc Appl*, 18:263–267, 1992.

[4] A. Bunsell et al. Benchmarking of strength models for unidirectional composites under longitudinal tension. *Compos Part A—Appl S*, 111:138–150, 2018.
[5] A. E. Scott et al. In situ fibre fracture measurement in carbon-epoxy laminates using high resolution computed tomography. *Compos Sci Technol*, 71:1471–1477, 2011.
[6] S. C. Garcea et al. Fibre failure assessment in carbon fibre reinforced polymers under fatigue loading by synchrotron X–ray computed tomography. *Compos Sci Technol*, 133:157 – 164, 2016.
[7] S. Pimenta and S. T. Pinho. Hierarchical scaling law for the strength of composite fibre bundles. *J Mech Phys Solids*, 61:1337–1356, 2013.
[8] S. Pimenta. A computationally efficient hierarchical scaling law to predict damage accumulation in composite fibre bundles. *Compos Sci Technol*, 146:210–225, 2017.
[9] M. Alves and S. Pimenta. A computationally–efficient micromechanical model for the fatigue life of unidirectional composites under tension–tension loading. *Int J Fatigue*, in press, 2018.
[10] B. W. Rosen. Tensile failure of fibrous composites. *AIAA Journal*, 2:1985–1991, 1964.
[11] G. W. Weibull. A statistical distribution function of wide applicability. *J Appl Math*, 18:293–297, 1951.
[12] A. Kelly and W. R. Tyson. Tensile properties of fibre–reinforced metals: copper/tungsten and copper/molybdenum. *J Mech Phys Solids*, 13:747–753, 2004.
[13] P. Paris and F. Erdogan. A critical analysis of crack propagation laws. *J Basic Eng, ASME*, December:528–534, 1963.
[14] I. J. Beyerlein and S. L. Phoenix. Stress concentrations around multiple fiber breaks in an elastic matrix with local yielding or debonding using quadratic influence superposition. *J Mech Phys Solids*, 44:1997–2039, 1996.
[15] S. Bai et al. Improving the adhesion between carbon fibres and an elastomer matrix using an acrylonitrile containing atmospheric plasma treatment. *Compos Interface*, 20:761–782, 2013.
[16] Toray Carbon Fibers America, Inc. Torayca T700G preliminary data sheet — Technical datasheet No. CFA 006, last accessed in June 2018.